ChemComm

COMMUNICATION

View Article Online
View Journal | View Issue

Cite this: *Chem. Commun.*, 2020, **56**, 4340

Received 31st December 2019,
Accepted 10th March 2020

DOI: 10.1039/c9cc10076h

rsc.li/chemcomm

Efficient organic solar cells based on a new "Y-series" non-fullerene acceptor with an asymmetric electron-deficient-core†

Fangfang Cai,‡[a] Can Zhu,‡[ab] Jun Yuan,*[a] Zhe Li,[a] Lei Meng,[b] Wei Liu,[a] Hongjian Peng,[a] Lihui Jiang,[a] Yongfang Li[b] and Yingping Zou*[a]

Herein, a new "Y-series" non-fullerene acceptor, Y21, bearing an asymmetric electron-deficient-core (DA′D) and fluorinated dicyanomethylene derivatives as flanking groups, was designed and synthesized for organic solar cell applications. Rather than being a perfect C_2 symmetric traditional "Y-series" acceptor, Y21 possesses an electron-withdrawing unit (A′) shifted from the center of DA′D, turning into an asymmetric molecular geometry. Photovoltaic devices based on PM6:Y21 can realize a high J_{sc} of 24.9 mA cm^{-2} and a PCE of 15.4%. Our work demonstrates a new way to tune the photoelectronic properties of the "Y-series" NFAs.

Organic solar cells (OSCs), in which the photoactive layer is composed of organic conjugated materials, have been considered as prospective technology because of the advantages in fabricating a device with light weight, mechanical flexibility, and solution processability.[1–7] In the last decade, fullerene derivatives have played a dominant role as electron acceptors due to their suitable electron affinity and isotropic electron transporting properties.[8–13] However, they have some inevitable drawbacks that impede their further application such as weak absorption in the visible-near infrared region, and limited tunability of their optical and electronic properties.[13–15] The recent emergence of "Y-series" non-fullerene acceptors (NFAs), typically Y6, has revitalized the field of OSCs, with their power conversion efficiency (PCE) rocketing from 11% to nearly 17% over the last year.[16–22] The Y-series NFAs with an A–DA′D–A configuration are a perfect combination of a ladder-type electron-deficient-core-based central fused core (DA′D), electron-accepting end-group (A) and two sp^2-hybridized nitrogen atoms in the pyrrole motif of the fused core in a C_2 symmetric manner.[23–26] Thus, the optoelectronic properties of Y-series NFAs can be easily tailored by chemical modification of either the terminal A unit or the alkyl side chain. Based on this molecular design strategy, a variety of high-performance Y-series NFAs have been constructed for photovoltaic applications.[16,19,24,27–29]

Although exciting progress has been made, the modification of the DA′D core was rarely reported. Moreover, the alkylated thieno[3,2-*b*]thiophene unit somehow increased the synthesis cost in traditional Y-series NFAs. Introducing the simple thiophene unit to replace the alkylated thieno[3,2-*b*]thiophene unit is the most intuitive approach to decrease the material cost of Y-series molecules. However, it was previously discussed that extending the absorption to an ideal bandgap (1.34 eV) derived from the Shockley–Queisser efficiency limit mode is one of the important principles for designing high photocurrent NFAs.[18,24,30–32]

In this study, we formulate a unidirectional replacement strategy to modify the DA′D core, diversifying the Y-series molecular structures. More importantly, the unidirectional replacement strategy may produce an asymmetric molecular structure which may have a large natural dipole moment.[33–35] The high dipole moment can strongly influence the molecular self-assembly between the neighboring molecules and resultantly reinforce the molecular packing. Consequently, a new asymmetric Y-series NFA, Y21, consisting of 5,11,12-tris(2-ethylhexyl)-8-hexyl-11,12-dihydro-5*H*-thieno[2′,3′:4,5]pyrrolo-[3,2-*g*]-thieno[2′,3′:4,5]thieno[3,2-*b*][1,2,3]triazolo[4,5-*e*]-indole group with 2-(5,6-difluoro-3-oxo-2,3-dihydro-1*H*-inden-1-ylidene)-malononitrile (fluorinated IC), was firstly reported by our group (Fig. 1a). Since the benzotriazole is flanked by the thiophene and alkylated thieno[3,2-*b*]thiophene unit, an asymmetric six-membered fused electron-deficient-core can be obtained. The 2-ethylhexyl side chains on the two nitrogen atoms of the fused center core can ensure good solubility and appropriate crystallinity, while the fluorinated end-group down-shifts the lowest unoccupied molecular orbital (LUMO) energy level and promotes the intermolecular interactions. Our result shows that the six-membered fused electron-deficient-core based acceptor Y21 also can determinate a broad absorption range with an optical gap (E_g^{opt}) of 1.35 eV.

[a] *College of Chemistry and Chemical Engineering, Central South University, Changsha 410083, P. R. China. E-mail: junyuan@csu.edu.cn, yingpingzou@csu.edu.cn*

[b] *Beijing National Laboratory for Molecular Sciences, Institute of Chemistry, Chinese Academy of Sciences, Beijing 100190, P. R. China*

† Electronic supplementary information (ESI) available. See DOI: 10.1039/c9cc10076h

‡ These two authors contributed equally to this work.

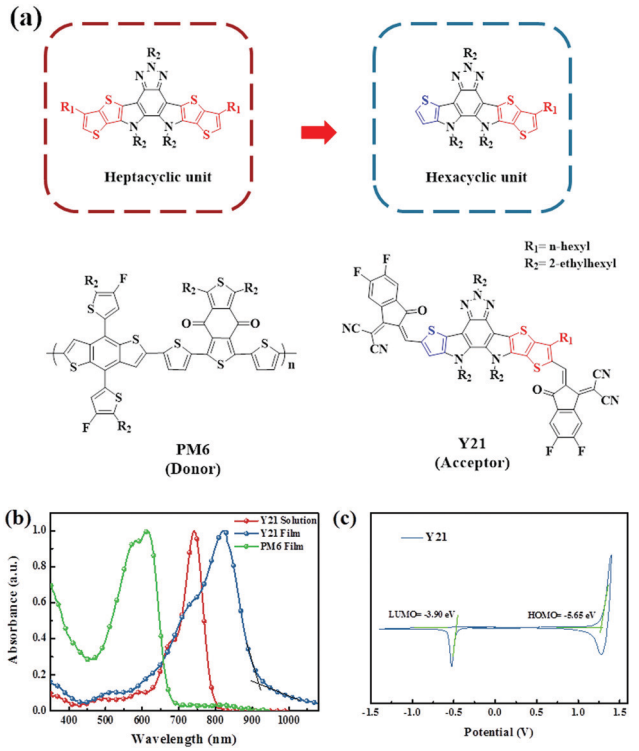

Fig. 1 (a) The design strategy of asymmetrical NFAs and their corresponding molecular structures; (b) normalized UV-vis absorption spectra of the solution and films of Y21 and PM6; (c) cyclic voltammograms of the Y21 film.

The OSCs based on Y21 blended with a medium bandgap polymer donor PM6 (Fig. 1a) exhibited a high PCE of 15.4% with an open-circuit voltage (V_{oc}) of 0.83 V, a short-circuit current density (J_{sc}) of 24.9 mA cm^{-2} and a fill factor (FF) of 74.4%.

The general synthetic route for the Y21 is shown in Scheme 1 and the detailed synthetic processes for the compounds are provided in the ESI.† Asymmetrical compound **2** was synthesized through the Stille coupling reaction by utilizing tributyl(thiophen-2-yl)stannane and tributyl(6-hexylthieno[3,2-*b*]thiophene-2-yl)stannane as raw materials. Then, the double intramolecular Cadogan reductive cyclization was carried out to convert the nitro groups of compound **2** into amino groups without further purification in the presence of triethyl phosphate, followed by the addition of 1-bromo-2-ethylhexane under alkaline conditions to obtain the ladder-type fused ring compound **4**. Dialdehyde compound **5** was prepared by the Vilsmeier–Haack reaction as an orange solid. Finally, the Knoevenagel condensation reaction of the fluorinated IC end-capping group with compound **5** yielded non-fullerene small molecules Y21. All intermediates were characterized by ^{1}H nuclear magnetic resonance (^{1}H NMR). Y21 was confirmed by ^{1}H NMR, ^{13}C NMR, and the high-resolution mass spectra (MS) (Fig. S1–S6, ESI†). Y21 readily dissolved in common organic solvents.

The normalized absorption spectra of Y21 and PM6 in dilute chloroform solution and thin film are shown in Fig. 1b, and the related data are presented in Table S1 (ESI†). In dilute chloroform solution, Y21 exhibited strong absorption in the 650–800 nm region with a maximum absorption peak at 741 nm.

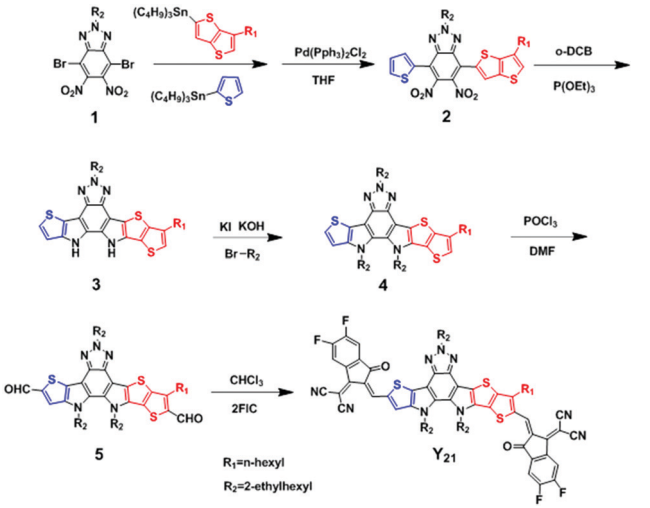

Scheme 1 Synthetic route of Y21.

From the solution to the solid state, the Y21 film showed a broader absorption range and a maximum absorption peak shifted from 741 to 823 nm, suggesting strong intermolecular interactions of Y21 in the solid state. Although the Y21 has only six fused aromatic rings, the maximum absorption peak of Y21 in the film is very similar to our previously reported molecule Y6 (821 nm, seven fused aromatic ring). The optical gap of Y21 estimated from the thin film (917 nm) is 1.35 eV. The electrochemical properties of Y21 were studied using cyclic voltammetry (CV) at a scanning rate of 20 mV s^{-1}. The highest occupied molecular orbital (HOMO) and lowest unoccupied molecular orbital (LUMO) energy levels of Y21 can be calculated according to the $E_{HOMO/LUMO} = -e(4.80 - E_{1/2,Fc/Fc^+} + E_{onset,ox/red})$ (eV) where $E_{1/2,Fc/Fc^+}$ is the redox potential of Fc/Fc$^+$ *vs.* Ag/AgCl in the measurement system. From Fig. 1c, the HOMO and LUMO of Y21 were estimated to be −5.65 eV and −3.90 eV, respectively. The optical and electrochemical data of Y21 are summarized in Table S1 (ESI†).

To investigate the photovoltaic performance of Y21, OSC devices with an inverted device structure of ITO/ZnO/active layer/MnO_3/Ag (Fig. 2a) were fabricated with PM6 as the donor material and Y21 as the acceptor material. To find the best condition for the active layer, the photovoltaic properties were systematically screened by varying the D/A ratio, processing additive concentration, and annealing temperatures. The ratio of D/A (weight ratio) was adjusted from 1 : 1 to 1 : 1.5, and the corresponding parameters are listed in Table S2 (ESI†). The device with a 1 : 1 ratio showed the best performance with a V_{oc} of 0.85 V, a J_{sc} of 24.3 mA cm^{-2}, a FF of 67.2% and a PCE of 13.9%. On the basis of 1 : 1 blend ratio, by thermal annealing at 100 °C for 10 min with 0.5% 1-chloronaphthalene (CN) as the additive, the PCE went up to 15.4% with a V_{oc} of 0.83 V, a J_{sc} of 24.9 mA cm^{-2}, and a FF of 74.4% (Table 1).

It is interesting to note that the Y21 devices possess similar V_{oc} and J_{sc} but different FF after optimizing the devices, which could be ascribed to the higher and balanced hole and electron mobilities of the blend films. Thus, the charge transport

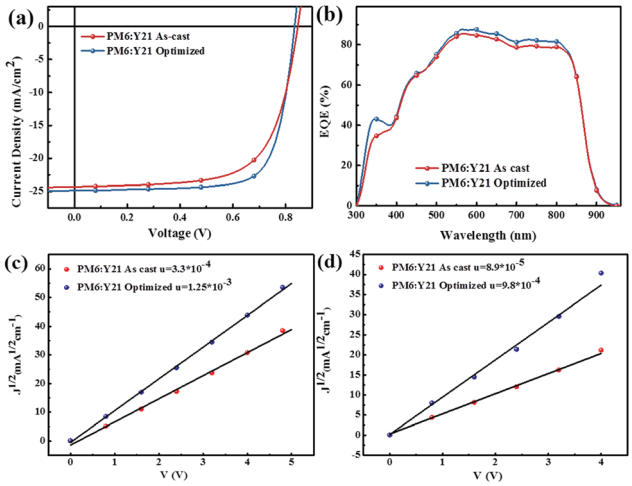

Fig. 2 (a) Current density *versus* voltage characteristics; (b) EQE curves of the devices; (c) *J*–*V* curves of the electron-only devices for the w/wo optimal active layer; (d) *J*–*V* curves of the hole-only devices for the w/wo optimal active layer.

Table 1 Photovoltaic performance of the OSCs based on PM6:Y21 (the average values for 15 devices in the brackets), under the illumination of AM 1.5G, 100 mW cm^{-2}

Active layer	V_{oc} (V)	J_{sc} (mA cm^{-2})	FF (%)	PCE (%)
PM6:Y21[a]	0.85	24.3	67.2	13.9 (13.7)
PM6:Y21[b]	0.83	24.9	74.4	15.4 (15.2)

[a] As-cast. [b] With 0.5% CN after thermal annealing.

properties in the PM6:Y21 blend were measured by the space-charge-limited current (SCLC) method using the hole-only and electron-only devices, respectively (Fig. 2c and d). For devices without any treatment, the electron and hole mobility (μ_e and μ_h) were 8.9 × 10^{-5} cm^2 V^{-1} s^{-1} and 3.3 × 10^{-4} cm^2 V^{-1} s^{-1} with a mobility ratio (μ_e/μ_h) of 3.7. Apparently, under the optimized conditions, the device exhibits a higher electron and hole mobility of 1.3 × 10^{-3}cm^2 V^{-1} s^{-1} and 9.8 × 10^{-4}cm^2 V^{-1} s^{-1} (μ_e/μ_h of 1.3).

The external quantum efficiency (EQE) curves are shown in Fig. 2b. The Y21 based devices show a broad photocurrent response from 300 to 900 nm and the maximum EQE plateau reached about 80% from 550 to 800 nm, indicating efficient photo harvesting and charge collection. The integrated photocurrents of the PM6:Y21 blend film with and without optimization from EQE spectra were 24.5 and 24.0 mA cm^{-2}, respectively, both of which are in good agreement with the J_{sc} values obtained (less than 2% error) from the corresponding *J*–*V* curves.

To evaluate the exciton dissociation and extraction processes in the Y21 based devices, the dependence of photocurrent density (J_{ph}) *versus* the effective voltage (V_{eff}) was measured. J_{ph} can be defined as $J_{ph} = J_{light} - J_{dark}$, where J_{light} and J_{dark} represent the photocurrent density under illumination and dark conditions, respectively. V_{eff} equals to $V_o - V_{bias}$, where V_o is the voltage when $J_{ph} = 0$ and V_{bias} is the applied external voltage bias. At high V_{eff} values (*i.e.*, $V_{eff} \geq 2$ V), J_{ph} reaches saturation (J_{sat}), suggesting that mobile charge carriers can rapidly move toward the corresponding electrodes with minimal recombination.[16] Thus, the exciton dissociation and extraction can be estimated using the J_{ph}/J_{sat} ratio. From Fig. S7 (ESI†), it can be seen that a high J_{ph}/J_{sat} value of 98.4% was achieved for Y21-based devices with an optimized active layer, which is slightly higher than that of the active layer without optimization (97.0%), indicating that a higher exciton dissociation and charge extraction process in treated devices contribute to its high J_{sc} and FF. Under the maximal power output conditions, the J_{ph}/J_{sat} values in Y21-based devices with and without an optimized active layer are still as high as 98.4% and 97.0%, respectively, indicating a considerably higher device performance after optimizing the active layer. We also measured the charge recombination behavior of the OSCs. The dependence of J_{sc} as a function of light intensity (P) was studied and modeled with the equation $J_{sc} \propto P_\alpha$. If all free charge carriers are swept out and collected at the electrodes prior to recombination, α tends to the limit 1.[21] In Fig. S8 (ESI†), the recombination parameters are 0.94 and 0.96 for the devices with as-cast and optimized blends, respectively, suggesting that bimolecular recombination is effectively suppressed during the operation of the optimized device.

The morphology of the PM6:Y21 blend films without and with 0.5% CN after thermal annealing was investigated by transmission electron microscopy (TEM). Fig. 3 shows the TEM images of the PM6:Y21 blend films prepared under different conditions. No distinct feature was found in the (as cast) blend films as shown in Fig. 3a. However, the addition of the CN additive and thermal annealing induce some suitable nanophase-segregated structures in the blends (Fig. 3b). The favorable phase size of the PM6:Y21 blend films can promote efficient charge separation and thus leads to high current density.

In conclusion, we have designed and synthesized a new NFA, Y21, with an asymmetric electron-deficient-core-based fused structure for use in OSCs. Y21 has good solubility in common solvents, a strong absorption profile ranging from 700 to 900 nm with an optical gap of 1.35 eV. In addition, by using the SCLC measurement method, high and balanced mobilities can be achieved in optimized PM6:Y21 blend films. Moreover, a suitable nanophase-segregated structure with an optimized size and preferred orientation is also observed in optimized PM6:Y21 blend films. Consequently, the asymmetrical Y21-based OSCs achieved a high PCE of 15.4% with a V_{oc} of 0.83 V, a J_{sc} of

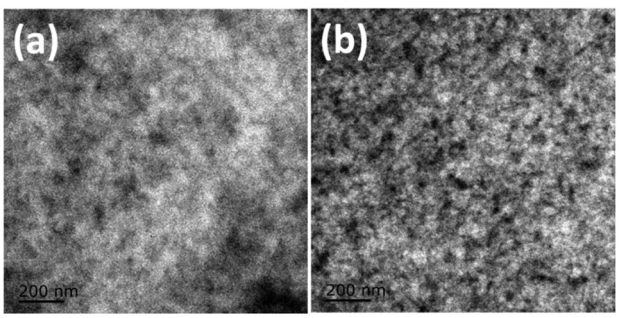

Fig. 3 TEM images of the PM6:Y21 blend films prepared under different conditions (a) as-cast and (b) with 0.5% CN after thermal annealing.

24.9 mA cm^{-2}, and a FF of 74.4%. This work reveals a new molecular design to modify the DA'D core and reports a new Y-series NFA for OSC applications.

This work has been financially supported by the National Natural Science Foundation of China (NSFC) (21875286), the National Key Research & Development Projects of China (2017YFA0206600), and the Science Fund for Distinguished Young Scholars of Hunan Province (2017JJ1029).

Conflicts of interest

There are no conflicts to declare.

Notes and references

1 G. Yu, J. Gao, J. C. Hummelen, F. Wudl and A. J. Heeger, *Science*, 1995, **270**, 1789–1791.
2 C. Yan, S. Barlow, Z. Wang, H. Yan, A. K. Y. Jen, S. R. Marder and X. Zhan, *Nat. Rev. Mater.*, 2018, **3**, 18003.
3 C. Cui and Y. Li, *Energy Environ. Sci.*, 2019, **12**, 675.
4 Y. W. Han, S. J. Jeon, H. S. Lee, H. Park, K. S. Kim, H. W. Lee and D. K. Moon, *Adv. Energy Mater.*, 2019, **9**, 1902065.
5 M. Kaltenbrunner, M. S. White, E. D. Glowacki, T. Sekitani, T. Someya, N. S. Sariciftci and S. Bauer, *Nat. Commun.*, 2012, **3**, 770.
6 G. Li, R. Zhu and Y. Yang, *Nat. Photonics*, 2012, **6**, 153–161.
7 B. Xu and J. Hou, *Adv. Energy Mater.*, 2018, **8**, 1800022.
8 D. Baran, T. Kirchartz, S. Wheeler, S. Dimitrov, M. Abdelsamie, J. Gorman, R. S. Ashraf, S. Holliday, A. Wadsworth, N. Gasparini, P. Kaienburg, H. Yan, A. Amassian, C. J. Brabec, J. R. Durrant and I. McCulloch, *Energy Environ. Sci.*, 2016, **9**, 3783–3793.
9 J. Huang, J. H. Carpenter, C. Z. Li, J. S. Yu, H. Ade and A. K. Jen, *Adv. Mater.*, 2016, **28**, 967–974.
10 H. Hoppe and N. S. Sariciftci, *J. Mater. Res.*, 2011, **19**, 1924–1945.
11 A. Wadsworth, Z. Hamid, M. Bidwell, R. S. Ashraf, J. I. Khan, D. H. Anjum, C. Cendra, J. Yan, E. Rezasoltani, A. A. Y. Guilbert, M. Azzouzi, N. Gasparini, J. H. Bannock, D. Baran, H. Wu, J. C. de Mello, C. J. Brabec, A. Salleo, J. Nelson, F. Laquai and I. McCulloch, *Adv. Energy Mater.*, 2018, **8**, 1801001.
12 M. T. Dang, L. Hirsch and G. Wantz, *Adv. Mater.*, 2011, **23**, 3597–3602.
13 L. Dou, J. You, J. Yang, C.-C. Chen, Y. He, S. Murase, T. Moriarty, K. Emery, G. Li and Y. Yang, *Nat. Photonics*, 2012, **6**, 180–185.
14 Y. Lin, J. Wang, Z. G. Zhang, H. Bai, Y. Li, D. Zhu and X. Zhan, *Adv. Mater.*, 2015, **27**, 1170–1174.
15 X. Meng, W. Zhang, Z. Tan, C. Du, C. Li, Z. Bo, Y. Li, X. Yang, M. Zhen, F. Jiang, J. Zheng, T. Wang, L. Jiang, C. Shu and C. Wang, *Chem. Commun.*, 2012, **48**, 425–427.
16 J. Yuan, Y. Zhang, L. Zhou, G. Zhang, H.-L. Yip, T.-K. Lau, X. Lu, C. Zhu, H. Peng, P. A. Johnson, M. Leclerc, Y. Cao, J. Ulanski, Y. Li and Y. Zou, *Joule*, 2019, **3**, 1140–1151.
17 Z. Zhou, W. Liu, G. Zhou, M. Zhang, D. Qian, J. Zhang, S. Chen, S. Xu, C. Yang, F. Gao, H. Zhu, F. Liu and X. Zhu, *Adv. Mater.*, 2019, **32**, 1906324.
18 J. Yuan, T. Huang, P. Cheng, Y. Zou, H. Zhang, J. L. Yang, S. Y. Chang, Z. Zhang, W. Huang, R. Wang, D. Meng, F. Gao and Y. Yang, *Nat. Commun.*, 2019, **10**, 570.
19 R. Qin, D. Wang, G. Zhou, Z.-P. Yu, S. Li, Y. Li, Z.-X. Liu, H. Zhu, M. Shi, X. Lu, C.-Z. Li and H. Chen, *J. Mater. Chem. A*, 2019, **7**, 27632–27639.
20 B. Fan, D. Zhang, M. Li, W. Zhong, Z. Zeng, L. Ying, F. Huang and Y. Cao, *Sci. China: Chem.*, 2019, **62**, 746–752.
21 Y. Lin, B. Adilbekova, Y. Firdaus, E. Yengel, H. Faber, M. Sajjad, X. Zheng, E. Yarali, A. Seitkhan, O. M. Bakr, A. El-Labban, U. Schwingenschlogl, V. Tung, I. McCulloch, F. Laquai and T. D. Anthopoulos, *Adv. Mater.*, 2019, **31**, 1902965.
22 L. Hong, H. Yao, Z. Wu, Y. Cui, T. Zhang, Y. Xu, R. Yu, Q. Liao, B. Gao, K. Xian, H. Y. Woo, Z. Ge and J. Hou, *Adv. Mater.*, 2019, **31**, 1903441.
23 B. Fan, Z. Zeng, W. Zhong, L. Ying, D. Zhang, M. Li, F. Peng, N. Li, F. Huang and Y. Cao, *ACS Energy Lett.*, 2019, 2466–2472.
24 Y. Cui, H. Yao, J. Zhang, T. Zhang, Y. Wang, L. Hong, K. Xian, B. Xu, S. Zhang, J. Peng, Z. Wei, F. Gao and J. Hou, *Nat. Commun.*, 2019, **10**, 2515.
25 T. Yan, W. Song, J. Huang, R. Peng, L. Huang and Z. Ge, *Adv. Mater.*, 2019, **31**, 1902210.
26 J. Kniepert, A. Paulke, L. Perdigón-Toro, J. Kurpiers, H. Zhang, F. Gao, J. Yuan, Y. Zou, V. M. Le Corre, L. J. A. Koster and D. Neher, *J. Appl. Phys.*, 2019, **126**, 205501.
27 R. Wang, J. Yuan, R. Wang, G. Han, T. Huang, W. Huang, J. Xue, H. C. Wang, C. Zhang, C. Zhu, P. Cheng, D. Meng, Y. Yi, K. H. Wei, Y. Zou and Y. Yang, *Adv. Mater.*, 2019, **31**, 1904215.
28 C. Sun, F. Pan, H. Bin, J. Zhang, L. Xue, B. Qiu, Z. Wei, Z. G. Zhang and Y. Li, *Nat. Commun.*, 2018, **9**, 743.
29 X. Li, F. Pan, C. Sun, M. Zhang, Z. Wang, J. Du, J. Wang, M. Xiao, L. Xue, Z. G. Zhang, C. Zhang, F. Liu and Y. Li, *Nat. Commun.*, 2019, **10**, 519.
30 A. Rose, *Phys. Rev.*, 1955, **97**, 1538–1544.
31 J. Z. Yao, T. Kirchartz, M. S. Vezie, M. A. Faist, W. Gong, Z. C. He, H. B. Wu, J. Troughton, T. Watson, D. Bryant and J. Nelson, *Phys. Rev. Appl.*, 2015, **4**, 044007.
32 S. Ullbrich, J. Benduhn, X. Jia, V. C. Nikolis, K. Tvingstedt, F. Piersimoni, S. Roland, Y. Liu, J. Wu, A. Fischer, D. Neher, S. Reineke, D. Spoltore and K. Vandewal, *Nat. Mater.*, 2019, **18**, 459–464.
33 H. Hu, K. Jiang, G. Yang, J. Liu, Z. Li, H. Lin, Y. Liu, J. Zhao, J. Zhang, F. Huang, Y. Qu, W. Ma and H. Yan, *J. Am. Chem. Soc.*, 2015, **137**, 14149–14157.
34 S. Feng, C. Zhang, Y. Liu, Z. Bi, Z. Zhang, X. Xu, W. Ma and Z. Bo, *Adv. Mater.*, 2017, **29**, 201703527.
35 W. Gao, M. Zhang, T. Liu, R. Ming, Q. An, K. Wu, D. Xie, Z. Luo, C. Zhong, F. Liu, F. Zhang, H. Yan and C. Yang, *Adv. Mater.*, 2018, **30**, 1800052.